

Collective Effects at Frictional Interfaces

O. M. Braun · Michel Peyrard · D. V. Stryzheus ·
Erio Tosatti

Received: 2 November 2011 / Accepted: 3 January 2012 / Published online: 20 January 2012
© Springer Science+Business Media, LLC 2012

Abstract We discussed the role of the long-range elastic interaction between the contacts inside an inhomogeneous frictional interface. The interaction produces a characteristic elastic correlation length $\lambda_c = a^2 E/k_c$ (where a is the distance between the contacts, k_c is the elastic constant of a contact, and E is the Young modulus of the sliding body), below which the slider may be considered as a rigid body. The strong inter-contact interaction leads to a narrowing of the effective threshold distribution for contact breaking and enhances the chances for an elastic instability to appear. Above the correlation length, $r > \lambda_c$, the interaction leads to screening of local perturbations in the interface, or to appearance of collective modes—frictional cracks propagating as solitary waves.

Keywords Boundary lubrication · Nanotribology · Viscosity · Master equation · Stick–slip

1 Introduction

Studies of sliding friction, a subject with great practical importance and with rich physics, attracted an increased interest during the last two decades [1, 2]. Tip-based experimental techniques as well as atomistic molecular dynamics (MD) computer simulations describe with considerable success the processes and mechanisms operating in atomic-scale friction. Much less is known with regard to meso- and macro-scale frictions, where one has to take into account that the frictional interface is inhomogeneous and generally complex. An immediate example is dry friction between rough surfaces. Even when the sliding surfaces are ideally flat but, for example, the substrates are not monocrystalline, or there is an interposed solid lubricant film consisting of misoriented domains, the frictional interface is again inhomogeneous. The same may be true even for liquid lubrication, if, under applied load, the lubricant solidifies making bridges due to Lifshitz–Slözov coalescence. In these cases, the so-called earthquake-like (EQ)-type models can be successfully applied [2–13]. In the EQ model, the two (top and bottom) mutually sliding surfaces are coupled by a set of contacts, representing, e.g., asperities, patches of lubricant, or 2D crystalline domains. A contact is assumed to behave as a spring of elastic constant k_c so long as its length is shorter than a critical value $x_s = f_s/k_c$; above this length, the contact breaks, to be subsequently restored with lower stress. The sliding kinetics of this model may be reduced to a master equation (ME), which allows an analytic study [8, 11, 12].

O. M. Braun · D. V. Stryzheus
Institute of Physics, National Academy of Sciences of Ukraine,
46 Science Avenue, Kiev 03028, Ukraine
e-mail: obraun.gm@gmail.com
URL: <http://www.iop.kiev.ua/~obraun>

M. Peyrard (✉)
Laboratoire de Physique de l'École Normale Supérieure de
Lyon, 46 Allée d'Italie, 69364 Lyon Cedex 07, France
e-mail: Michel.Peyrard@ens-lyon.fr

E. Tosatti
International School for Advanced Studies (SISSA),
Via Bonomea 265, 34136 Trieste, Italy

E. Tosatti
International Centre for Theoretical Physics (ICTP),
P.O. Box 586, 34014 Trieste, Italy

E. Tosatti
CNR-IOM Democritos National Simulation Center,
Via Bonomea 265, 34136 Trieste, Italy

In the simplest approach, the slider is treated as a rigid body. Owing to the non-rigidity of the substrates, however, several length scales naturally appear in the problem. First, different regions of the interface will exhibit different displacements. If the length λ_L is such that, for distances $r \gg \lambda_L$, the displacements are independent, then it is known as the Larkin–Ovchinnikov length [14]. It was shown [15] that, for the contact of stiff rough solid surfaces, λ_L may reach disproportionately large values $\sim 10^{100,000}$ m. Second, deformations of the solid substrates lead to the elastic interaction between the contacts. Elasticity will correlate variations of forces on the nearest contacts over some length λ_c known as the elastic correlation length [16]. Third, displacements in one region of the slider will be felt in other regions on the distance scale set by of a screening length λ_s . Finally, the breaking of one contact may stimulate neighboring contacts to break too (the so-called concerted, or cascade jumps), following which an avalanche-like collective motion of different domains of the interface may appear [5].

In this article, we discuss collective effects in the frictional interface and propose approaches to treat them from different viewpoints. In particular, our aim is to clarify the following questions: (i) what is the law of interaction between the contacts? (ii) at which scale can the slider be considered as a rigid body, or what is the coherence distance λ_c within which the motion of contacts is strongly correlated? (iii) whether the interaction effects can be incorporated in the ME approach? (iv) how does the interaction modifies the interface dynamics? (v) what is the screening length λ_s ? and (vi) when do avalanche motion of contacts (a self-healing crack) appear, and what is the avalanche velocity?

The article is organized as follows. The EQ model, its description with the ME approach, and the elastic instability responsible for the stick–slip motion are introduced in Sect. 2. The interaction between contacts is studied in Sect. 3. An approach to incorporate the interaction between contacts into the ME approach in a mean-field fashion is described in Sect. 4. The role of interaction at the meso/macro-scale is considered in Sect. 5. Finally, discussions in Sect. 6 conclude the article.

2 EQ Model, ME, and Elastic Instability

2.1 The EQ Model

In the EQ model, the sliding interface is treated as a set of N contacts which deforms elastically with the average rigidity k_c . The i th contact connects the slider and the substrate through a spring of shear elastic constant k_i . When the slider is moved, the position of each contact

point changes, the contact spring elongates (or shortens), so that the slider experiences a force $-F = \sum f_i$ from the interface, where $f_i = k_i x_i$ and $x_i(t)$ is the shift of the i th junction from its unstressed position. The contacts are assumed to be coupled “frictionally” to the slider. As long as the force $|f_i|$ is below a certain threshold f_{si} , the i th contact moves together with the slider. When the force exceeds the threshold, the contact breaks and a rapid local slip takes place, during which the local stress drops. Subsequently, the junction is pinned again in a less-stressed state with f_{bi} , and the whole process repeats itself. Thus, with every contact, we associate the threshold value f_{si} and the backward value f_{bi} , which take random values from the distributions $\tilde{P}_c(f)$ and $\tilde{R}(f)$ respectively. When a contact is formed again (re-attached to the slider), new values for its parameters are assigned. The EQ model was studied numerically in a number of studies [3–10], typically with the help of the cellular automaton numerical algorithm.

2.2 The ME Approach

Rather than studying the evolution of the EQ model by numerical simulation, it is possible to describe it analytically [8, 11, 12]. Let $P_c(x)$ be the normalized probability distribution of values of the stretching thresholds x_{si} at which contacts break; it is coupled with the distribution of threshold forces by the relationship $P_c(x)dx = \tilde{P}_c(f)df$, i.e., the corresponding distributions are coupled by the relationship $P_c(x) \propto x\tilde{P}_c[f(x)]$, where $f \propto x^2$ [11]. We assume that the distribution $P_c(x)$ has a dispersion Δx_s centered at $x = x_c$.

To describe the evolution of the model, we introduce the distribution $Q(x; X)$ of the contact stretchings x_i when the sliding block is at position X . Evolution of the system is described by the integro-differential equation (known as the ME, or the kinetic equation, or the Boltzmann equation) [8, 11]

$$\left[\frac{\partial}{\partial X} + \frac{\partial}{\partial x} + P(x) \right] Q(x; X) = R(x)\Gamma(X), \tag{1}$$

where

$$\Gamma(X) = \int_{-\infty}^{\infty} d\xi P(\xi)Q(\xi; X) \tag{2}$$

and

$$P(x) = P_c(x)/J_c(x), \quad J_c(x) = \int_x^{\infty} d\xi P_c(\xi). \tag{3}$$

Then, the friction force (the total force experienced by the slider from the interface) is given by $(k_c = \langle k_i \rangle)$

$$F(X) = Nk_c \int_{-\infty}^{\infty} dx x Q(x; X). \tag{4}$$

In the steady state corresponding to smooth sliding, the ME reduces to

$$dQ(x)/dx + P(x)Q(x) = R(x)\Gamma, \tag{5}$$

which has the solution:

$$Q_s(x) = \mathcal{N}E_P(x) \left[1 + \Gamma \int_{0^+}^x d\xi R(\xi)/E_P(\xi) \right], \tag{6}$$

where \mathcal{N} is the normalization constant, $\int_0^\infty dx Q_s(x) = 1$, and

$$E_P(x) = \exp[-U(x)], \quad U(x) = \int_0^x d\xi P(\xi). \tag{7}$$

2.3 Elastic Instability

The solution of the ME [8, 11] shows that, when a *rigid* slider begins to move adiabatically, $\dot{X} > 0$, it experiences from the interface a friction force $F_\infty(X) < 0$. Initially, $|F_\infty|$ grows roughly linearly with X , $|F_\infty| \approx K_s X$ where $K_s = Nk_c$ is the total elastic constant (“rigidity”) of the interface, until it reaches a value $\sim F_s - \Delta F_s$, where $F_s \approx K_s x_c$ and $\Delta F_s \approx K_s \Delta x_s$. Gradually, however, contacts begin to break and reform, slowing down the increase of $|F_\infty|$ and then inverting the slope through a displacement Δx_s until almost all contacts have been reborn. Successively, the process repeats itself with a smaller amplitude until, owing to increasing dispersion of breaking and reforming processes, the force asymptotically levels off and attains a position-independent steady-state kinetic friction value with smooth sliding.

According to Newton’s third law, the external driving force $F_d = K(vt - X)$, which causes the displacement X (where K is the slider rigidity and v is the driving velocity), is compensated by the force from the interface, $F_d = F(X)$. Smooth sliding is always attained with a rigid slider. It persists for a nonrigid slider as well, so long as the pulling spring stiffness is large enough, $K > K^*$, where

$$K^* = \max F'_\infty(X), \quad F'_\infty(X) \equiv dF_\infty(X)/dX. \tag{8}$$

When conversely the slider or the pulling spring elastic constant are soft enough ($K < K^*$), there is a mechanical instability. The driving force F_d cannot be compensated by the force from the interface, and the slider motion becomes unstable at X_c , where X_c is the (lowest) solution of $F'_\infty(X) = K$ (for details see Refs. [8, 11]). The mechanical instability yields stick–slip frictional motion of the slider.

Thus, the regime of motion—either stick–slip for $K \ll K^*$ or smooth sliding for $K \gg K^*$ —is controlled by the effective stiffness parameter: $K^* \sim K_s x_c / \Delta x_s$. When all contacts are identical, $\Delta x_s = 0$ so that $K^* = \infty$, then one always obtains a stick–slip motion.

2.4 Material Parameters

It is useful here, before proceeding with the analytic and numerical developments necessary to answer the questions posed in the Introduction, to review the practical significance and magnitude of the model parameters.

2.4.1 Elastic Constant of the Slider

The slider (shear) elastic constant K is equal to $K = [E/2(1 + \sigma)][L_x L_y / H]$, where L_x , L_y , and H are the slider dimensions, E and σ are the substrate Young modulus and Poisson ratio, respectively [17]. For example, for a steel slider of Young’s modulus $E = 2 \times 10^{11}$ N/m², Poisson’s ratio $\sigma = 0.3$, and the size $L_x \times L_y \times H = 1$ cm \times 1 cm \times 1 cm, we obtain $K = 10^9$ N/m.

2.4.2 Rigidity of the Interface Contacts

Now, we characterize the typical magnitudes of the contact stretching length x_c and stiffness k_c . Assume the slider and the substrate to be coupled by $N = L_x L_y / a^2$ contacts, and that the contacts have a cylindrical shape of (average) radius r_c with a distance a between the contacts. It is useful to introduce the dimensionless parameter $\gamma_2 = r_c / a$, which may be estimated as follows [1]. Consider a cube of linear size L on a table. The weight of the cube $F_l = \rho L^3 g$ (ρ is the mass density and $g = 9.8$ m/s²) must be compensated by forces from the contacts, $F_l = N r_c^2 \sigma_c$, where σ_c is the plastic yield stress. Then, $\gamma_2^2 = (N r_c^2) / (Na^2) = (\rho L^3 g) / (\sigma_c L^2)$, or $\gamma_2 = (\rho L g / \sigma_c)^{1/2}$. Taking $L = 1$ cm, $\rho = 10$ g/cm³, and $\sigma_c = 10^9$ N/m² (steel), we obtain $\gamma_2 = 10^{-3}$ which should be typical for a contact of rough stiff surfaces. For softer materials, and especially for a lubricated interface, the values of γ_2 would be much larger, e.g., $\gamma_2 = 0.1$.

The second dimensionless parameter $\gamma_1 = k_c / Ea$ characterizes the stiffness of the contacts. To estimate γ_1 , assume again contacts with the shape of a cylinder of radius r_c and length h (h is the thickness of the interface). Suppose in addition that one end of a contact (“column”) is fixed, and a shear force f is applied to the free end. This force will lead to the displacement $x = f / k_c$ of the end, where $k_c = 3E_c I / h^3$, E_c is the Young modulus of the contact material, and $I = \pi r_c^4 / 4$ is the moment of inertia of the cylinder [17]. In this way, we obtain $k_c = (3\pi/4)(E_c r_c) (r_c/h)^3$, so that $\gamma_1 = (3\pi/4)(E_c a^3 / Eh^3)(r_c/a)^4 = \gamma_0 \gamma_2^4$ with

$\gamma_0 = (3\pi/4)(E_c/E)(a/h)^3$. For the contact of rough surfaces, where $E_c = E$ and $a \gtrsim h$, we have $\gamma_0 \gtrsim 1$, while for lubricated interfaces where $E_c \ll E$, one would expect $\gamma_0 \lesssim 1$.

An estimate of characteristic values [1] leads to $r_c \sim (10^{-3} \div 10^{-2})a$. Thus, for the steel slider considered above, taking $r_c = h = 1 \mu\text{m}$ and intercontact spacing $a = 3 \times 10^2 r_c$, we obtain $N = 10^3$ and $k_c = 5 \times 10^5 \text{ N/m}$, so that the global stiffness of the interface is $K_s = 5 \times 10^8 \text{ N/m}$.

2.4.3 Stick–Slip Versus Smooth Sliding

As mentioned above in Sect. 2.3, the regime of motion (either stick–slip or smooth sliding) is controlled by the parameter $K^* \sim K_s x_c / \Delta x_s$. For the steel slider considered above, estimates gave $K = 10^9 \text{ N/m}$ and $K_s = 5 \times 10^8 \text{ N/m}$. Thus, if the surfaces are rough so that $\Delta x_s \sim x_c$, then $K > K^*$ and one should typically get smooth sliding. Stick slip appears further disfavored if we consider a realistic $P_c(x)$ distribution. For all cases mentioned in Introduction—the contact of rough surfaces (both for elastic or plastic asperities), the contact of polycrystal (flat) substrates, and the case of lubricated interface, when the lubricant melted during a slip, solidifies and forms bridges at stick—the distribution $P_c(x)$ is rather wide with a large concentration of small-threshold contacts [11], which makes the value of K^* very small. Thus, the theory predicts that most systems do not undergo an elastic instability and should not therefore exhibit stick–slip. This conclusion contradicts everyday experience as well as careful experiments, where stick–slip is pervasive. As suggested by EQ simulations [13], the discrepancy is most likely caused by ignoring the elastic interaction between the contacts.

The role of interaction is considered in the next sections. First, however, we need to define the form and parameters of the interaction between contacts.

3 Interaction Between Contacts

Friction is not a simple sum of individual contact properties. The collective behavior of the contacts is important. Recently, Persson [18–22] developed a contact mechanics theory based on the fractal structure of surfaces to determine the actual contact area at all length scales, which determines the friction coefficient. This approach includes the presence of multiple contacts and leads to the correct low-threshold limit: $\tilde{P}_c(f \rightarrow 0) = 0$. Persson found that the distribution of normal stresses σ ($\sigma > 0$) at the interface may approximately be described by the expression $P_\sigma(\sigma) \propto \exp[-(\sigma - \bar{\sigma})^2 / \Delta\sigma^2] - \exp[-(\sigma + \bar{\sigma})^2 / \Delta\sigma^2]$, where $\bar{\sigma}$ is the nominal squeezing pressure, the distribution

width is given by $\Delta\sigma = E^* \mathcal{R}^{1/2}$ (E^* is the combined Young modulus of the substrates, $E^{*-1} = E_1^{-1} + E_2^{-1}$ where $E_{1,2}$ are the Young moduli of the two substrates), and the parameter \mathcal{R} is determined by the roughness of the contacting surfaces, $\mathcal{R} = (4\pi)^{-1} \int d\mathbf{q} q^3 \int d^2x \langle h(\mathbf{x})h(\mathbf{0}) \rangle e^{-i\mathbf{q}\mathbf{x}}$. Assuming that a local shear threshold is directly proportional to the local normal stress, $f \propto \sigma$, we finally obtain the distribution, which is characterized by a low concentration of small shear thresholds, $\tilde{P}_c(f) \propto f$ at $f \rightarrow 0$, and a fast decaying tail, $\tilde{P}_c(f) \propto \exp(-f^2/f^{*2})$ at $f \rightarrow \infty$, i.e., now the peaked structure of the distribution is much more pronounced.

However, an important aspect which has to be included is the redistribution of the forces when some contacts deform or break. A concerted motion of contacts may emerge only due to interaction between the contacts which occurs through the deformation of the bulk in the directions parallel to the average contact plane. It is this aspect that we want to consider here. For the elastic interaction, a qualitative picture is presented in Fig. 1 (left). When a contact acts on the surface at $r = 0$ with a force f , it produces a displacement field $u(r) \propto r^{-1}$ which affects other contacts (Fig. 1a)—similar to the Coulomb potential for a point charge [17]. However, if there are two surfaces, then the same contact acts on the second surface with the opposite force $-f$ and, if the two surfaces are in contact, the resulting displacement field should fall as $u(r) \propto r^{-3}$ (Fig. 1b)—similar to the dipole–dipole potential for a screened point charge near a metal surface [23]. The question thus is the form of the interaction for the multi-contact interface (Fig. 1c). We will show that the interaction between the contacts has a crossover from the r^{-1} slow Coulomb decay at short distances to the faster dipole–dipole one at large distances.

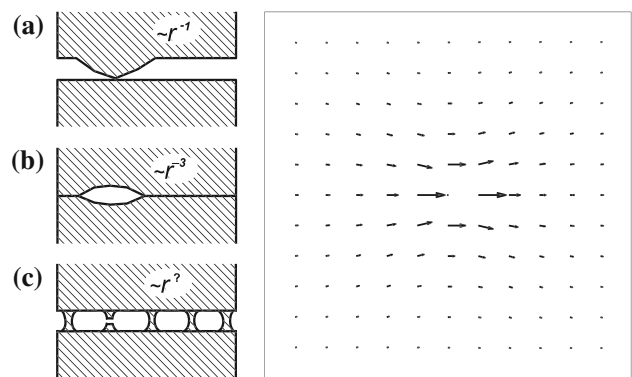


Fig. 1 Left decaying of the displacement field at the interface (schematic): (a) for a single contact $u(r) \propto r^{-1}$, (b) for a single hole $u(r) \propto r^{-3}$, and (c) for the array of contacts. Right change of forces on contacts when the central contact is removed ($\gamma_1 = 0.06$)

3.1 Analytics

Let us consider an array of N elastic contacts (springs) with coordinates $\mathbf{r}_i \equiv \{x_i, y_i, 0\}$, $i = 1, \dots, N$, between the two (top and bottom) substrates. If the interface is in a stressed state, the contacts act on the top substrate with forces $\mathbf{f}_i \equiv \{f_{ix}, f_{iy}, f_{iz}\}$. These contact forces produce displacements $\mathbf{u}_i^{(\text{top})}$ of the (bottom) surface of the top substrate. The $3N$ -dimensional vectors $\mathbf{U}^{(\text{top})} \equiv \{\mathbf{u}_i^{(\text{top})}\}$ and $\mathbf{F}_t \equiv \{\mathbf{f}_i\}$ are coupled by the linear relationship $\mathbf{U}^{(\text{top})} = \mathbf{G}^{(\text{top})}\mathbf{F}_t$. Elements of the elastic matrix $\mathbf{G}^{(\text{top})}$ (known also as the elastic Green tensor) for a semi-infinite isotropic substrate were given by Landau and Lifshitz [17]:

$$\begin{aligned} G_{ix,jx} &= g(r_{ij})[2(1 - \sigma) + 2\sigma x_{ij}^2/r_{ij}^2] \\ G_{ix,jy} &= 2g(r_{ij})\sigma x_{ij}y_{ij}/r_{ij}^2 \\ G_{ix,jz} &= -g(r_{ij})(1 - 2\sigma)x_{ij}/r_{ij} \\ G_{iz,jx} &= -G_{ix,jz} \\ G_{iz,jz} &= 2g(r_{ij})(1 - \sigma), \end{aligned} \tag{9}$$

where $x_{ij} = x_i - x_j$, $g(r) = (1 + \sigma)/(2\pi Er)$, and σ and E are the Poisson ratio and Young modulus of the top substrate, respectively.

In the equilibrium state, the forces that act from the contacts on the bottom substrate, must be equal to $\mathbf{F}_b = -\mathbf{F}_t$ according to Newton’s third law. These forces lead to displacements of the (top) surface of the bottom substrate, $\mathbf{U}^{(\text{bottom})} = -\mathbf{G}^{(\text{bottom})}\mathbf{F}_t$. The elements of the bottom Green tensor $\mathbf{G}^{(\text{bottom})}$ are defined by the same expressions (9) except the xz elements for which $G_{ix,jz}^{(\text{bottom})} = -G_{ix,jz}^{(\text{top})}$ (if the substrates are identical, the z displacements are irrelevant). Thus, the relative displacements at the interface due to elastic interaction between the contacts are determined by

$$\mathbf{U} \equiv \mathbf{U}^{(\text{top})} - \mathbf{U}^{(\text{bottom})} = -\mathbf{G}\mathbf{F}, \tag{10}$$

where $\mathbf{F} = -\mathbf{F}_t$ and $\mathbf{G} = \mathbf{G}^{(\text{top})} + \mathbf{G}^{(\text{bottom})}$.

On the other hand, the forces and displacements are coupled by the diagonal matrix (the contacts’ elastic matrix) \mathbf{K} , $K_{ix,j\beta} = k_{ix} \delta_{ij} \delta_{\alpha\beta}$ ($\alpha, \beta = x, y, z$):

$$\mathbf{F} = \mathbf{K}(\mathbf{U}_0 + \mathbf{U}), \tag{11}$$

where \mathbf{U}_0 defines a given stressed state (because of linearity of the elastic response, final results should not depend of \mathbf{U}_0). The total force at the interface, $\mathbf{f} = \sum_i \mathbf{f}_i$, must be compensated by external forces applied to the substrates, e.g., by the force $\mathbf{f}^{(\text{ext})} = \mathbf{f}$ applied to the top surface of the top substrate if the bottom surface of the bottom substrate is fixed.

Combining Eqs. 10 and 11, we obtain $\mathbf{F} = \mathbf{K}(\mathbf{U}_0 - \mathbf{G}\mathbf{F})$, or

$$\mathbf{F} = \mathbf{B}\mathbf{K}\mathbf{U}_0, \quad \text{where } \mathbf{B} = (\mathbf{1} + \mathbf{K}\mathbf{G})^{-1}. \tag{12}$$

If one changes the contact elastic matrix, $\mathbf{K} \rightarrow \mathbf{K} + \delta\mathbf{K}$, then the interface forces should change as well,

$\mathbf{F} \rightarrow \mathbf{F} + \delta\mathbf{F}$. From Eq. 12 we have $\delta\mathbf{F} = (\delta\mathbf{B})\mathbf{K}\mathbf{U}_0 + \mathbf{B}(\delta\mathbf{K})\mathbf{U}_0$. Then, $\delta\mathbf{B}$ may be found from the equation $\delta[\mathbf{B}(\mathbf{1} + \mathbf{K}\mathbf{G})] = (\delta\mathbf{B})(\mathbf{1} + \mathbf{K}\mathbf{G}) + \mathbf{B}(\delta\mathbf{K})\mathbf{G} = 0$. Therefore, finally, we obtain as follows:

$$\delta\mathbf{F} = \mathbf{B}\delta\mathbf{K}(\mathbf{1} - \mathbf{G}\mathbf{B}\mathbf{K})\mathbf{U}_0. \tag{13}$$

Above we have assumed that $\delta\mathbf{K}$ is small. If it is not small, we have to use the expression $\delta\mathbf{F} = \mathbf{B}\delta\mathbf{K}(\mathbf{1} - \mathbf{G}\mathbf{B}\tilde{\mathbf{K}})\mathbf{U}_0$, where $\tilde{\mathbf{K}} = (\mathbf{1} + \delta\mathbf{K}\mathbf{G}\mathbf{B})^{-1}(\mathbf{K} + \delta\mathbf{K})$.

Now, if we remove the i^* th contact by putting $\delta k_{ix} = -k_{ix}\delta_{ii^*}$ and then calculate the resulting change of forces on other contacts, we can find a response of the interface to the breaking of a single contact as a function of the distance $\mathbf{r} = \mathbf{r}_i - \mathbf{r}_{i^*}$ from the broken contact.

3.2 Numerics

Equation 13 may be solved numerically by standard methods of matrix algebra. We explore an idealized array of identical contacts, $k_{ix} = k_c$ and $(\mathbf{U}_0)_{ix} = u_0\delta_{xx}$ for all i , organized in a square 89×89 lattice with spacing $a = 1$, with the broken contact i^* at the center of the lattice. For singular terms of the Green function (9) we apply a cutoff at $r_{ii} = r_c$. Numerical results depend on two dimensionless parameters. The first is $\gamma_1 = k_c/E^*a$, which determines the stiffness of the array of contacts relative the substrates (here $E^* = E_{\text{top}}^{-1} + E_{\text{bottom}}^{-1}$). The second parameter $\gamma_2 = r_c/a$ characterizes a single contact (or the density of asperities). For the Poisson ratio we took a typical value $\sigma = 0.3$. A typical distribution of breaking induced force changes is shown in Fig. 1 (right).

The numerical results for the x -component of dimensionless force $\delta f = \delta F_x/(k_c u_0)$ are presented in Fig. 2. The function $\delta f(r)$ exhibits a crossover from a slow Coulomb like decay $\delta f(r) \propto r^{-1}$ at short distances $r \ll \lambda_c$ to the fast dipole–dipole like decay $\delta f(r) \propto r^{-3}$ at large distances $r \gg \lambda_c$. The near and far zones are separated by the *elastic correlation length* λ_c first introduced by Caroli and Nozieres [16]. It may be estimated in the following way: the stiffness of the “rigid block” $K \sim E\lambda_c$ should be compensated by that of the interface, $K \sim k_c(\lambda_c a)^2$ (stiffness of one contact times the number of contacts). This leads to

$$\lambda_c \approx a/\gamma_1 = a^2 E/k_c. \tag{14}$$

The rigid slider corresponds to the limit $E \rightarrow \infty$, or $\gamma_1 \rightarrow 0$. Therefore, the slider may be considered as a rigid body (e.g., in MD simulation), if its size is smaller than λ_c . For the steel slider considered in Sect. 2.4, estimation gives $\lambda_c a \sim 10^2$. Up to distance λ_c the contacts strongly interact. If the i th contact breaks and its stretching changes on $|\delta x_i| \approx x_c$, then the force on the j th contact at a distance $r_{ij} < \lambda_c$ away, changes by $\delta f_j \approx \tilde{\kappa} k_c a \delta x_i / r_{ij}$, where the dimensionless parameter $\tilde{\kappa} < 1$ characterizes the strength of interaction

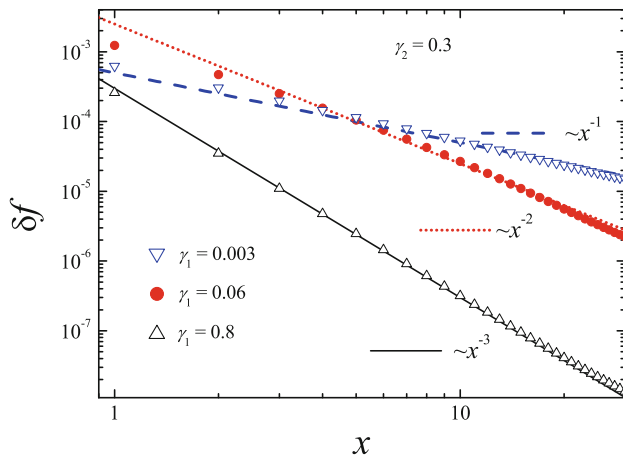


Fig. 2 (Color online) Dependence of the change of forces $\delta f(r)$ on the distance x from the broken contact for three values of the interface stiffness: $\gamma_1 = 0.003$ (blue down triangles, dashed line), 0.06 (red solid circles, dotted line) and 0.8 (black up triangles, solid line) at fixed value of $\gamma_2 = 0.3$ ($\sigma = 0.3$). The lines show the corresponding power laws

(numerics gives $\tilde{\kappa} \sim 10^{-3}$). In the near zone, $r \ll \lambda_c$, the interaction between the contacts may be accounted for within the ME approach in a mean-field fashion as described in the next Sect. 4. At larger distances, different regions of the slider will undergo different displacements. Therefore, in the far zone, $r \gg \lambda_c$, we must take into account the elastic deformation of the slider.

4 Nearby Contacts: Mean Field Approach

4.1 EQ Model with Interaction Between the Contacts

Let us now include the dynamical interaction between the contacts. When a contact breaks, the now unsustainable shear stress must be redistributed among the neighboring contacts. We assume that, because of elastic interaction between the contacts i and j , the forces acting on these contacts have to be corrected as $f_i \rightarrow f_i - \Delta f_{ij}$ and $f_j \rightarrow f_j + \Delta f_{ij}$, where $\Delta f_{ij} = k_{ij}(x_j - x_i)$ in linear approximation. For example, let at the beginning the contacts be relaxed, $x_j(0) = x_i(0) = 0$. Due to sliding motion, all stretchings grow together, so that still $\Delta f_{ij} = 0$. At some instant t , let the j th contact break, $x_j(t) \rightarrow 0$, with the i th contact still stretched, $x_i(t) > 0$. Clearly, as the j th contact breaks, the force on the i th contact increases, $\Delta f_{ij}(t) = -k_{ij}x_i(t) < 0$. The amplitude of interaction decreases with the distance r from the broken contact as $\Delta f \propto r^{-1}$ at short distances $r < \lambda_c$. Neglecting the anisotropy of interaction, we assume that $k_{ij} = \tilde{f}/|r_{ij}|$, where \tilde{f} is a parameter.

We simulated a triangular lattice of $N = 60 \times 68 = 4080$ contacts with periodic boundary conditions and

lattice constant $a = 1$, with an average contact spring constant $k_c = 1$, and radius of interaction $\lambda_c = 3a$ or $\lambda_c = 5a$. We assumed $f_{bi} = 0$ and a rectangular shape of the distribution $P_c(x)$, i.e., $P_c(x) = P_{c0}(x) = (2\Delta x_s)^{-1}$ for $|x - x_s| < \Delta x_s$ and 0 otherwise, which admits an exact solution for noninteracting contacts [11] (more realistic distributions give the same results).

Figures 3 and 4 show the result of simulations for different values of the dimensionless strength of the interaction

$$\kappa = \tilde{f}/(k_c x_c), \tag{15}$$

where $x_c = \int dx x P_{c0}(x)$ is the average stretching of the initial threshold distribution (for the rectangular distribution $x_c = x_s$). These results yield the following conclusions. *First*, in the steady state, the interaction causes a narrowing of the final distribution $Q_s(x)$. At high interaction strength κ , the distribution approaches a narrow Gaussian. *Second*, the drop of frictional force $F(X)$ at the onset of sliding (at $X \sim x_c$) gets steeper and steeper as κ grows. Therefore, contact interactions reinforce elastic instability. *Third*, above a critical interaction strength, $\kappa \geq \kappa_c \sim 0.1$, a multiplicity of contacts break simultaneously at the onset of sliding, and there is an avalanche, where the force $F(X)$ drops abruptly. The average avalanche size may be estimated similarly as done in Ref. [5].

While the full EQ model may be only studied numerically, it is always useful to have analytical results, even if only of qualitative level. In what follows we show that the main EQ results may be reproduced within the ME approach by using “effective” $P_c(x)$ and $R(x)$ distributions

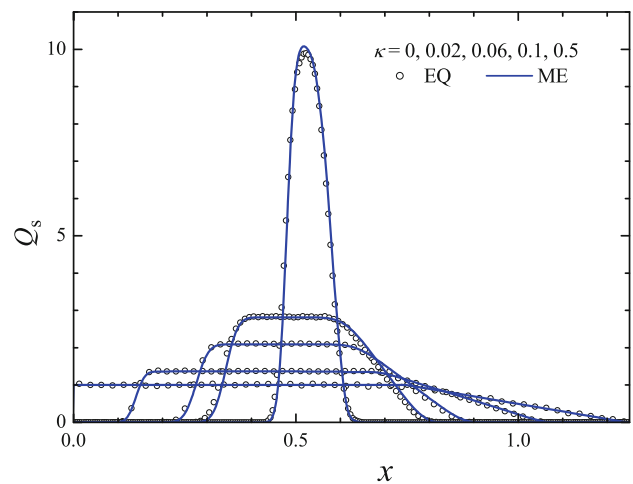


Fig. 3 (Color online) The steady-state distribution $Q_s(x)$ for the rectangular threshold distribution $P_{c0}(x)$ with $x_s = 1$ and $\Delta x_s = 0.25$ and different values of the interaction strength $\kappa = 0, 0.02, 0.06, 0.1,$ and 0.5 . The EQ simulations (dotted) are compared with the ME results (solid curves)

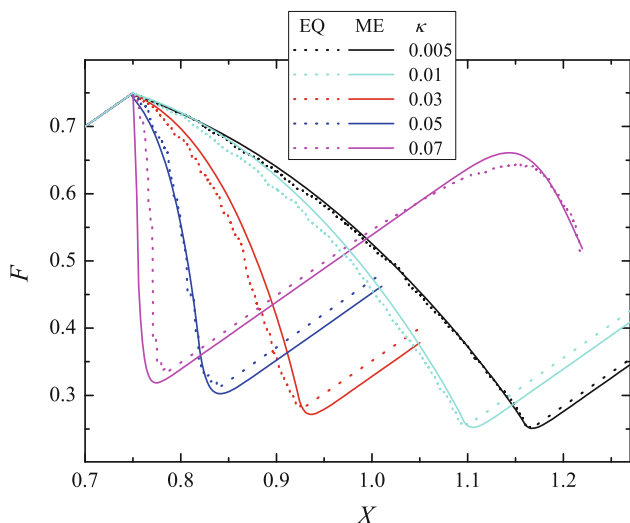


Fig. 4 (Color online) Onset of sliding: the initial part of the dependence of the friction force F on the slider displacement X for different strength of interaction $\kappa = 0.005$ (black), 0.01 (cyan), 0.03 (red), 0.05 (blue), and 0.07 (magenta). Dotted curves show the results of EQ simulation, and solid curves, the mean-field ME approach. The threshold distribution $P_{c0}(x)$ has the rectangular shape with $x_s = 1$ and $\Delta x_s = 0.25$

defined in a mean-field fashion. In this section, the ME equation is only used to reproduce the EQ results. This is, however, useful because it provides an additional understanding of the results, as the effective distributions obtained in this analysis, provide a description of the collective effects affecting the contacts in terms of simple functions.

4.2 Smooth Sliding

Using the steady-state solution of the ME, and Eqs. 6 and 7, one may approximately recover the functions $P_c(x)$ and $R(x)$ if the stationary distribution $Q_s(x)$ is known. Indeed, for small x , where $P(x)$ is close to zero, the left-hand side of $Q_s(x)$ allows us to find $R(x)$ as $R(x) \propto Q'_s(x)$ (see Eq. 5), while the right-hand side of $Q_s(x)$, where $x \sim x_c$ and the contribution of $R(x)$ to the shape of the steady-state distribution is negligible, gives us [11] $P_c(x) \propto P(x)Q_s(x) \propto -Q'_s(x)$. Thus, differentiating the function $Q_s(x)$ obtained in the EQ simulation, we may guess shapes of the effective distributions $P_c(x)$ and $R(x)$ which, when substituted in the ME, would produce a solution $Q_s(x)$ close to that obtained in the EQ simulation.

Using the simulation results, let us suppose that the detached contacts form again with nonzero stretchings, i.e., that the distribution $R(x)$ is shifted to positive stretching values,

$$R(x) = G(x - \alpha x_c, \gamma x_c), \tag{16}$$

where $G(x, \sigma)$ is the Gaussian distribution with zero mean and standard deviation σ ,

$$G(x, \sigma) = \frac{1}{\sigma\sqrt{2\pi}} \exp\left(-\frac{x^2}{2\sigma^2}\right). \tag{17}$$

At the same time, we suppose that the effective threshold distribution $P_c(x)$ shrinks and shifts with respect to the original (“noninteracting”) one,

$$P_h(x) = \beta P_{c0}[\beta(x - \alpha x_c)]. \tag{18}$$

Let us moreover take its convolution with the Gaussian function (17), $P_c(x) = P_h \otimes G \equiv \int d\xi P_h(x - \xi)G(\xi, \gamma\sqrt{2}x_c)$.

The results of this procedure for the rectangular distribution $P_{c0}(x)$ are shown in Fig. 3. We see that, with a proper choice of the parameters α , β and γ , the ME solutions $Q_s(x)$ perfectly fits the numerical EQ results (for the parameters α , β , and γ in Fig. 3 we used expressions $\beta = 1 + b_1\kappa$, $\alpha = b_2\kappa/\beta$, and $\gamma = b_3\alpha - b_4\alpha^2$ with the coefficients $b_1 = 18$, $b_2 = 9.6$, $b_3 = 0.142$, and $b_4 = 0.232$). Results of similar quality were also obtained for other simulated cases, e.g., for larger radius of the interaction or for wider threshold distribution $P_{c0}(x)$.

The dependences of the fitting parameters α , β , and γ on the dimensionless strength of interaction κ may be found in the following way. To begin with, for noninteracting contacts initially $\alpha = \gamma = 0$ and $\beta = 1$. It is reasonable to expect that in the lowest approximation $\alpha, \gamma \propto \kappa$ and $\beta - 1 \propto \kappa$. Indeed, because the shift of the effective distribution $P_c(x)$ appears because of the interaction, $\alpha f_c = \sum_j \Delta f_{ij}$, at small κ we have approximately

$$\alpha \sim 0.5a^{-2} \int_0^{\lambda_c} d^2 r \kappa x_c / |r| = \pi \kappa \lambda_c x_c / a^2. \tag{19}$$

At large κ , however, α has to saturate, e.g., as $\alpha \propto \kappa/\beta$, because the shift cannot be larger than x_c , i.e., $\alpha < 1$. Then, because the distribution $P_c(x)$ shrinks from both sides, we have $b_1 \sim 2b_2$.

Thus, the interaction makes the threshold distribution $P_c(x)$ narrower by a factor β and shifts its center to the left-hand side, $x_c \rightarrow vx_c$, where $v = \alpha + \beta^{-1}$ changes from 1 to 0.5 as the interaction strength κ increases from zero to infinity.

4.3 Onset of Sliding

The beginning of motion when started from the relaxed configuration, $Q(x; 0) = \delta(x)$, cannot be explained by the approach used above, because the effective distribution $P_c(x)$ is “self-generated” during smooth sliding, i.e., it can be applied only when the process of contacts breaking–reattachment is continuously operating. Nevertheless, the initial part of the $F(X)$ dependence may still be described

by the effective ME approach, but with the modified “forward” threshold distribution given by the expression

$$P_{ci}(x) = \mathcal{N}x^{\epsilon_0}P_{c0}[\beta_0(x - \alpha_0x_c)], \tag{20}$$

where \mathcal{N} is a normalization factor, $\int_0^\infty dxP_{ci}(x) = 1$. The parameter α_0 is now defined so as to keep the lowest boundary unshifted, $\beta_0(x_{\text{fix}0} - \alpha_0x_c) = x_{\text{fix}0}$ with $x_{\text{fix}0} = x_L = x_s - \Delta x_s$, so that $\alpha_0 = (x_{\text{fix}0}/x_c)(1 - \beta_0^{-1})$. The “backward” distribution $R(x)$ is still defined by Eq. 16 with the same parameters as above.

Numerics shows that, with a proper choice of the fitting parameters β_0 and ϵ_0 for a given value of κ , the initial part of the function $F(X)$ may be reproduced with quite high accuracy. Moreover, for a rather wide range of κ values, the EQ simulation results may be reproduced by the ME approach with a reasonable accuracy using only three fitting parameter c_1, c_2 and κ_c , if the parameters β_0 and ϵ_0 in Eq. 20 are given by the expressions $\beta_0 = 1 + c_1\kappa/(1 - \kappa/\kappa_c)$ and $\epsilon_0 = c_2(\beta_0 - 1)$, where the parameter κ_c corresponds to the critical “breakdown” interaction strength when many contacts begin to break simultaneously. For $\kappa > \kappa_c$, the drop of $F(X)$ becomes jump-like, so that $K^* = \infty$ and stick–slip will appear for any stiffness of the slider $K < \infty$. Note that the value of κ_c may be estimated from the equation $\alpha x_c \sim \Delta x_s$.

For the rectangular shape of the distribution $P_{c0}(x)$ the result of this procedure is demonstrated in Fig. 4 (the fitting parameters are $c_1 = 33.9, c_2 = 3.0$ and $\kappa_c = 0.074$).

Of course, the $P_{ci}(x)$ function, Eq. 20, can describe only the initial part of the $F(X)$ dependence, when $F(X)$ grows, reaches the first maximum and then decreases. To simulate the whole dependence $F(X)$, one would have to involve the evolution of $P_c(x)$ with sliding distance, e.g., as some “aging” process $P_{ci}(x) \rightarrow P_c(x)$ (see Ref. [11]) with the initial distribution $P_{c,\text{ini}}(x) = P_{ci}(x)$ and the final one $P_{c,\text{fin}}(x) = P_c(x)$.

4.4 Stick–Slip Versus Smooth Sliding

As was mentioned above, stick–slip appears as a result of elastic instability which is controlled by the relation between the slider stiffness K and the effective interface stiffness K^* . For noninteracting contacts $K^* \approx K_s x_c / \Delta x_s$; because typically $\Delta x_s \sim x_c$, estimates give $K^* \lesssim K$ so that stick–slip should never appear. The interaction between contacts strongly enhances the elastic instability thus making stick–slip much more probable. Indeed, because of the effective shrinking of the threshold distribution, the parameter K^* increases roughly as $K^* \rightarrow K^*_{\text{eff}} \sim \beta_0 K^*$, i.e., the effective interface stiffness K^*_{eff} grows with the strength of interaction κ , and the elastic instability can now appear. For example, for a realistic threshold distribution the dependence of K^*_{eff} on the strength of interaction κ is shown in Fig. 5.

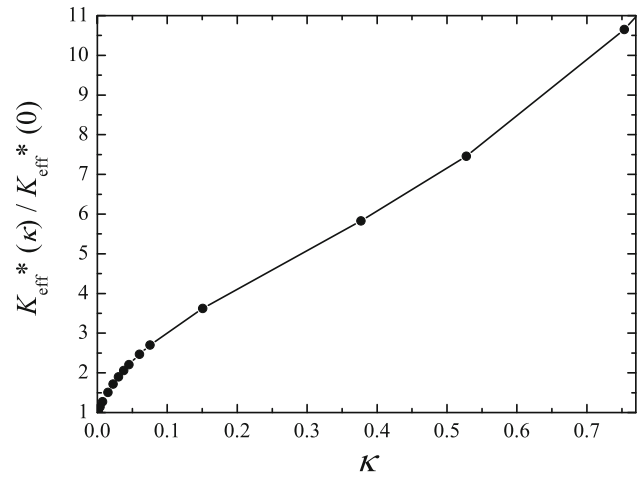


Fig. 5 The effective interface stiffness K^*_{eff} (normalized on the noninteracting value) as a function of the strength of interaction κ for the realistic threshold distribution $P_{c0}(x) = (2/x_s) u^3 e^{-u^2}$, $u \equiv x/x_s$ with $x_s = 1$, when $K^*/K_s = 0.179$

The strength of interaction between the contacts may be found as $\kappa \approx \bar{\kappa}a/x_c$, where realistic values of the dimensionless parameter $\bar{\kappa}$ are of the order $\bar{\kappa} \sim 10^{-3}$; taking $a \sim (10^2 \div 10^3)r_c$ and $x_c = r_c$, we obtain $\kappa \sim 0.1 \div 1$ which gives $\beta_0 \sim 3 \div 13$ according to Fig. 5.

5 Far Zone: Meso/macroscopic Friction

At the *mesoscopic scale*, i.e., on distances $r \gg \lambda_c$, the substrate must be considered as deformable. Let us split the frictional area into (rigid) blocks of size λ_c . In a general 3D model of the elastic slider, the n th λ_c -block is characterized by a coordinate X_n , and its dynamics is described by the ME for the distribution functions $Q_n(u_n; X_n)$. A solution of these MEs gives the interface forces $F_n(X_n)$. Then, the transition from the discrete numbering of blocks to a continuum interface coordinate r is trivial: $n \rightarrow r, Q_n(u_n; X_n) \rightarrow Q[u; X(r); r], P_n(u) \rightarrow P(u; r), \Gamma_n(X_n) \rightarrow \Gamma[X(r); r], F_n(X_n) \rightarrow F[X(r); r]$ (here r is a two-dimensional vector at the interface), and the ME now takes the form:

$$\frac{\partial Q[u; X(r); r]}{\partial X(r)} + \frac{\partial Q[u; X(r); r]}{\partial u} + P(u)Q[u; X(r); r] = \delta(u)\Gamma[X(r); r], \tag{21}$$

where we assumed that, for the sake of simplicity, the contacts are reborn with zero stretching, $R(u) = \delta(u)$, and

$$\Gamma[X(r); r] = \int d\xi P(\xi)Q[\xi; X(r); r]. \tag{22}$$

Equations 21, 22 should be completed with the elastic equation of motion for the sliding body (we assume isotropic slider)

$$\ddot{\mathbf{u}} + \eta\dot{\mathbf{u}} = G_1\nabla^2\mathbf{u} + G_2\nabla(\nabla \cdot \mathbf{u}), \tag{23}$$

where $\mathbf{u}(\mathbf{R})$ is the 3D displacement vector in the slider ($\mathbf{R} = \{x, y, z\}$), η is the intrinsic damping in the slider, $G_1 = E/2(1 + \sigma)\rho = c_t^2$ and $G_2 = G_1/(1 - 2\sigma)\rho = c_l^2 - c_t^2$, E , σ and ρ are the Young modulus, Poisson ratio and mass density of the slider correspondingly, and $c_l(c_t)$ is the longitudinal (transverse) sound speed. Equation 23 should be solved with corresponding boundary and initial conditions. In particular, at the interface (the bottom plane of the slider, where $z = 0$ and $\{x, y\} = r$) we must have $\mathbf{u}_x = X(r)$, $\mathbf{u}_y = \mathbf{u}_z = 0$, and the shear stress should equal $F[X(r); r]/\lambda_c^2$, where the friction force acting on the λ_c -block from the interface,

$$F[X(r); r] = N_\lambda k_c \int duuQ[u; X(r); r], \tag{24}$$

should be obtained from the solution of Eq. 21 [here $N_\lambda = (\lambda_c/a)^2$].

Equations 21–24 form the complete set of equations which describes evolution of the large scale tribological system; in a general case it has to be solved numerically. However, a qualitative picture may be obtained analytically. The interface dynamics depends on whether or not the λ_c -blocks undergo the elastic instability, i.e., on the ratio of the stiffness of the λ_c -block $K_\lambda \approx (2c_l^2 + 3c_t^2)\rho\lambda_c$ (as follows from the discretized version of Eq. 23) and the effective critical stiffness parameter of the interface $K_{\lambda, \text{eff}}^* = \beta_0 K_\lambda^*$, where $K_\lambda^* \sim K_{\lambda_s} x_c / \Delta x_s$ and $K_{\lambda_s} = N_\lambda k_c$. If the elastic instability does not appear, then a local perturbation at the interface relaxes, spreading over an area of size λ_s —the screening length considered below in Sect. 5.1. In the opposite case, when the elastic instability does emerge (locally), it may propagate through the interface. Below in Sect. 5.2 we consider a simplified one-dimensional version, which allows us to get some analytical results and a rather simple simulation approach (such a model is also supported by the fact that the largest forces near the broken contact are just ahead/behind it according to Fig. 1). Recall that the interaction between the λ_c -blocks is weaker than in the short-range zone, it follows the law $\delta f \propto r^{-3}$ which determines, e.g., the block–block interaction strength κ_λ in Eq. 26 below (although the interaction is power-law, we may consider the nearest neighbors only, because excitations at the interface, such as “kinks” introduced in Sect. 5.2, are localized excitations, and the role of long-range character of the interaction reduces to modification of their parameters [24]).

5.1 Elastic Screening Length

Let us assume that the slider is split in λ_c -blocks (rigid blocks) and consider the block–block interaction in a

mean-field fashion (analogously to methods used in soft matter, see Refs. [25–27]). Due to sliding of neighboring blocks, the forces acting on contacts in the n th λ_c -block get an additional shift. This effect may be accounted with the help of a substitution $f_n \rightarrow f_n + \Delta f_n$, $\Delta f_n = \sum_{m \neq n} f_m \times \text{Prob}(m \rightarrow \text{broken}) \times \Pi_{mn} \approx x_c \sum_{m \neq n} f_m \Gamma_m \Pi_{mn}$ (recall that the sum is over the λ_c -blocks here), or approximately

$$f_n \rightarrow \left[1 + x_c \sum_{m \neq n} \Gamma_m(X_m) \Pi_{mn} \right] f_n, \tag{25}$$

where $\Gamma_m(X_m) = \int du P_m(u) Q_m(u; X_m)$ so that $N_\lambda \Gamma_m(X_m)$ is the number of broken contacts in the m th λ_c -block per its unit displacement, and

$$\Pi_{mn} \approx N_\lambda \kappa_\lambda (\lambda_c/r_{mn})^3 \tag{26}$$

describes the dimensionless (i.e., normalized on f_s) elastic interaction between the λ_c -blocks separated by the distance r_{mn} . In this way the force is given by $f_s \Pi$; the numerical constant $\kappa_\lambda \sim \bar{\kappa} a / \lambda_c$ depends on the substrate and interface parameters.

Let us introduce the dimensionless variable $\varepsilon_n = x_c \sum_{m \neq n} \Gamma_m(X_m) \Pi_{mn}$. The shift of forces in the n th block due to broken contacts in the neighboring blocks may be accounted by a renormalization of the rate:

$$P_n(u) \rightarrow P_n[(1 + \varepsilon_n)u]. \tag{27}$$

Indeed, when contacts in the neighboring blocks break, then the forces in the given block increase, $\varepsilon_n > 0$, and the contacts in the given block should start to break earlier, i.e., their threshold distribution effectively shifts to lower values.

Making the transition from discrete sliding blocks to a continuum sliding interface, $\Pi_{mn} \rightarrow \Pi(r' - r)$ and $\varepsilon_n \rightarrow \varepsilon(r)$, we obtain a ME of the form:

$$\frac{\partial Q[u; X(r); r]}{\partial X(r)} + \frac{\partial Q[u; X(r); r]}{\partial u} + P([1 + \varepsilon(r)]u)Q[u; X(r); r] = \delta(u)\Gamma[X(r); r], \tag{28}$$

where we again assumed that the contacts are reborn with zero stretchings, $R(u) = \delta(u)$,

$$\varepsilon(r) = x_c \lambda_c^{-2} \int_{|r'-r| \geq \lambda_c} d^2 r' \Gamma[X(r'); r'] \Pi(r' - r) \tag{29}$$

and

$$\Gamma[X(r); r] = \int d\xi P([1 + \varepsilon(r)]\xi) Q[\xi; X(r); r]. \tag{30}$$

In the long-wave limit, when $|d\varepsilon(r)/dr| \ll \varepsilon(r)/\lambda_c$, we may assume that the interface is locally equilibrated, i.e., the distribution of forces on contacts is close to the

steady-state solution of the ME, $Q[u; X(r); r] \approx Q_s(u; r)$, which depends parametrically on the coordinate r through the function $\varepsilon(r)$ entered into the expression for the rate $P([(1 + \varepsilon(r))u])$. The stationary solution of the ME is known analytically [11], and we may find the function (30), $\Gamma(r) = [1 + \varepsilon(r)]/x_c$. Together with Eq. 29 this gives a self-consistent equation on the function $\varepsilon(r)$:

$$\varepsilon(r) = \lambda_c^{-2} \int_{|r'-r| \geq \lambda_c} d^2r' [(1 + \varepsilon(r'))\Pi(r' - r)]. \quad (31)$$

Taking into account the interaction of the nearest neighboring λ_c -blocks only and expanding $\varepsilon(r)$ in Taylor series, we obtain the equation:

$$\varepsilon(r) = \Pi_0 \left[1 + \varepsilon(r) + \frac{1}{2} \lambda_c^2 \varepsilon''(r) \right], \quad (32)$$

where $\Pi_0 = v\Pi(\lambda_c) = vN_\lambda \kappa_\lambda \sim v\bar{\kappa}\lambda_c/a$ and $v = 2 \div 4$ is the number of the nearest neighbors. Writing $\varepsilon(r) = \varepsilon_0 + \Delta\varepsilon(r)$, where $\varepsilon_0 = \Pi_0/(1 - \Pi_0)$, Eq. 32 may be rewritten as

$$\lambda_s^2 \Delta\varepsilon''(r) = \Delta\varepsilon(r), \quad (33)$$

where $\lambda_s = \lambda_c(\varepsilon_0/2)^{1/2}$ is the characteristic screening length in the sliding interface.

From the known analytic steady-state solution of the ME [12], we may predict the dependence of screening length on temperature and sliding velocity. In particular, if $T > 0$, then $\lambda_s \propto v^{-1/2} \rightarrow \infty$ as $v \rightarrow 0$ in agreement with the results of Ref. [28].

5.2 Frictional Crack as a Solitary Wave

In the frictional interface, sliding begins at some weak place and then expands throughout the interface. Such a situation is close to the one known in fracture mechanics as the mode II crack, when the shear is applied along the fracture plane. In friction, a crack first opens, evolves (propagates, grows, extends) during some “delay” time τ , but then it either expands throughout the whole interface, or it will *close* because of the load. Below we consider the latter scenario, when one solid slips over another due to motion of the so-called self-healing crack [29–32]—a wave or “bubble” of separation moving like a crease on rug [33]. Our plan is to adopt ideas from fracture mechanics, adapt them to the friction problem, and then reduce it to the Frenkel–Kontorova (FK) model [24] to describe collective motion of contacts in the frictional interface.

When one of the “collective contacts” (the λ_c -block) breaks, it may initiate a chain reaction, with contacts breaking domino-like one after another. This scenario may

be described accurately by reducing the system of contacts to a FK-like model. Recall that the FK model describes a chain of harmonically interacting atoms subjected to the external periodic potential $V_{\text{sub}}(x)$ of the substrate. If the atoms are additionally driven by an external force f , then the equations of motion for the atomic coordinates u_n take the form:

$$m\ddot{u}_n + m\eta\dot{u}_n - g(u_{n+1} + u_{n-1} - 2u_n) + V'_{\text{sub}}(u_i) = f,$$

where m is the atomic mass, g is the strength of elastic interaction between the atoms, and η is an effective damping coefficient which describes dissipation phenomena such as the excitation of phonons *etc.* in the substrate. The main advantage of using the FK model is that its dynamics is well documented [24]. Mass transport along the chain is carried by kinks (antikinks)—local compressions (extensions) of otherwise commensurate structure. The kink is a well-defined topologically stable excitation (quasiparticle) characterized by an effective mass m_k which depends on the kink velocity $v_k, m_k = m_{k0} (1 - v_k^2/c^2)^{-1/2}$ (the relativistic Lorentz contraction of the kink width when its velocity approaches the sound speed c). Therefore, the maximal kink velocity $v_{k,\text{max}} = c$. In the discrete chain, kinks move in the so-called Peierls–Nabarro (PN) potential, whose amplitude is much lower than that of the primary potential $V_{\text{sub}}(x)$. Therefore, the kink motion is activated over these barriers, and its minimal velocity $v_{k,\text{min}}$ is nonzero. The steady-state kink motion is determined by the energy balance: the incoming energy (because of action of the external driving force f) should go to creation of new “surfaces” (determined by the amplitude of the substrate potential) plus excitation of phonons by the moving kink (described by the phenomenological damping coefficient η), so that $v_k(f) = f/(m_k\eta)$.

5.2.1 FK–ME Model

Thus, let us consider a chain of λ_c -contacts (“atoms” of mass $m = \rho\lambda_c^3$), coupled harmonically with an elastic constant g , driven externally through a spring of elastic constant K with the end moving with a velocity v . Using the discretized version of Eq. 23, the elastic constants may be estimated as $g \approx 2\lambda_c\rho c_T^2$ and $K \approx \lambda_c\rho c_T^2$. The λ_c -contacts are coupled “frictionally” with the bottom substrate; the latter is described by the nonlinear force $F_s(u)$. The equation of motion of the discrete chain is

$$m\ddot{u}_n + m\eta\dot{u}_n - g(u_{n+1} + u_{n-1} - 2u_n) + F_s(u_n) + Ku_n = f, \quad (34)$$

where the driving force is given by $f(t) = Kvt$. The substrate force $F_s(u)$ is found from the solution of the ME for

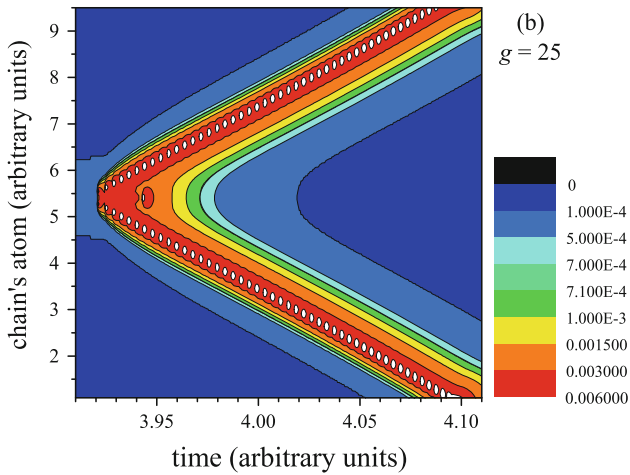


Fig. 6 (Color online) Color map of atomic velocities for a typical evolution of the chain of contacts. The nearest neighboring contacts interact elastically with the constant $g = 25$. The interaction with the substrate is modeled by the function $F_s(u) = k_c[\tanh(u) + 1.5e^{-u} \sin(3u)]$ with $k_c = 1$ defined for $0 \leq u < u_c = 1$ and periodically prolonged for other values of u . All contacts are driven through the springs of the elastic constant $K = 0.07$, their ends moving with the velocity $v = 10^{-4}$. The motion is overdamped ($m = 1, \eta = 100$). To initiate the breaking, two central contacts interact with the substrate with smaller values of the elastic constant, $k_c = 0.5$

the rigid λ_c -block. A typical evolution of the chain is shown in Fig. 6.

The general case may only be investigated numerically. Let us first consider a simplified case, when $F_s(u)$ has the sawtooth shape, i.e., it is defined as

$$F_s(u) = k_c u \quad \text{for } 0 \leq u < u_c \tag{35}$$

and periodically prolonged for other values of u . We assume that f is approximately constant during kink motion (otherwise, the kink will accelerate during its motion along the chain); this is correct if the change of the driving force $\Delta f = K v \Delta t$ during kink motion through the chain, $\Delta t = L/v_k$ (L is the chain length and v_k is kink velocity), is much lower than $k_c u_c$, or $K/k_c \ll (v_k/v)(u_c/L)$.

Let us define the function $\mathcal{F}(u) = F_s(u) + Ku - f$. The degenerate ground states of the chain are determined by the equation $\mathcal{F}(u) = 0$. Let the right-hand side ($n \rightarrow \infty$) of the chain be unrelaxed, $k_c u_R + Ku_R = f$, or

$$u_R = f/(k_c + K), \tag{36}$$

while the left-hand side ($n \rightarrow -\infty$) has already undergone relaxation, $k_c(u_L - u_c) + Ku_L = f$, or

$$u_L = (f + k_c u_c)/(k_c + K). \tag{37}$$

Thus, the FK-like model of friction (the FK–ME model) is described by Eqs. 34 and 35 with the boundary conditions given by Eqs. 36 and 37.

5.2.2 Continuum-Limit Approximation

Let the system be overdamped ($\ddot{u} = 0$); later on, we shall remove this restriction. In the continuum-limit approximation, $n \rightarrow x = na$ ($a = 1$), the motion equation takes the form:

$$m\eta u_t - a^2 g u_{xx} + \mathcal{F}(u) = 0, \quad \mathcal{F}(u)|_{x \rightarrow \pm\infty} = 0. \tag{38}$$

We look for a solution in the form of a wave of stationary profile (the solitary wave), $u(x, t) = u(x - v_k t)$, so that $u_t = -v_k u'$ and $u_{xx} = u''$. In this case Eq. 38 takes the form:

$$m\eta v_k u' + a^2 g u'' = \mathcal{F}(u), \tag{39}$$

which may be solved analytically by standard methods [34].

A solution of Eq. 39 with these boundary conditions exists only for a certain value of the kink velocity v_k , defined by the equation

$$(m\eta v_k)^2 = g a^2 (k_c + K)(2 - \beta)^2 / (\beta - 1), \tag{40}$$

where $\beta = k_c J(k^* - K)$ and $k^* = f/u_c$. The solitary-wave solution exists for forces $f_{\min} < f < f_{\max}$ only. The minimal force which supports the kink motion—the Griffith threshold—is given by

$$f_{\min} = \left(\frac{1}{2}k_c + K\right)u_c. \tag{41}$$

The maximal force, for which a kink may exist, is given by

$$f_{\max} = (k_c + K)u_c; \tag{42}$$

at higher forces, the barriers of $F_s(u)$ are degraded, the stationary ground states disappear, and the whole chain must switch to the sliding state.

From Eq. 40, we can find the kink velocity as a function of the driving force. At low velocities,

$$v_k \approx (f - f_{\min})/m_k \eta, \tag{43}$$

where we introduced the effective kink (crack) mass

$$m_k = m \sqrt{\frac{4a}{u_c} \frac{g}{k_c} \left(1 + \frac{K}{k_c}\right)}, \tag{44}$$

while at $f \rightarrow f_{\max}$ the velocity tends to infinity,

$$m\eta v_k \approx \sqrt{\frac{g k_c (k_c + K) a^2 u_c}{(f_{\max} - f)}}. \tag{45}$$

The latter limit should be corrected by taking into account inertia effects. The term $m\ddot{u}$ in Eq. 34 gives $m v_k^2 u''$ for the solitary-wave solution, so it can be incorporated if we substitute in the above equations $g \rightarrow g_{\text{eff}} = g(1 - v_k^2/c_0^2)$, where $c_0 = (g a^2/m)^{1/2}$ is the sound speed along the chain. The high-velocity limit now takes the form:

$$v_k \approx c_0 / \sqrt{1 + \frac{m\eta^2(f_{\max} - f)}{k_c(k_c + K)u_c}} \tag{46}$$

5.2.3 Simulations

The continuum-limit approximate is accurate for the case of strong interaction between the contacts, $g \gg 1$; in the opposite limit one has to resort to computer simulation. We solved Eq. 34 by the Runge–Kutta method. As the initial state, we took the chain of length N (typically $N = 3 \times 10^3$ or 3×10^4) with periodic boundary conditions and all contacts relaxed, but the threshold breaking value for two central contacts was taken lower than for the other contacts. Then the driving force increases because of stage motion, two central contacts break first and initiate two solitary waves of subsequent contact breaking which propagate in the opposite directions through the chain. The value k'_c of the lower threshold of the central contacts determines the driving force and therefore the kink velocity; the lower this threshold, the lower the threshold force for the motion to start [34]. As soon as the kink motion is initiated, the k_c -values of the central contacts are restored to the same value as for other contacts (otherwise these contacts will act as a source of creation of new pairs of kinks), and we begin to move the stage in the opposite direction, $v > 0 \rightarrow v_b < 0$, so that the driving force linearly decreases with time (see Fig. 7b), the average chain velocity $\langle \dot{u}_i \rangle = N^{-1} \sum_i \dot{u}_i$ decreases as well (Fig. 7c) until the motion stops (Fig. 7a). Also, such an algorithm allows us to find the dependence of the kink velocity determined as

$$v_k = n_k^{-1} N (\langle \dot{u}_i \rangle - \bar{v}), \tag{47}$$

where $n_k = 2$ is the number of moving kinks in the chain and $\bar{v} = \dot{u}_{L,R} = v_b K / (k_c + K)$ is the background velocity, on the driving force f . These dependences are presented in Fig. 8; they agree well with that predicted by Eqs. 40 and 43.

Contrary to the continuum-limit approximation, in the discrete chain of contacts the kink oscillates during motion (see Fig. 7d)—the well-known discreteness effect of the FK model due to existence of the PN barriers f_{PN} . The stronger the elastic interaction between the contacts, the larger the kink “width” and the smaller the kink oscillations (compare Fig. 8a and b). The amplitude of oscillations also depends on the shape of the “substrate potential” [24]—it is larger for a sawtooth potential $F_s(u)$, but smaller for a smoother shapes. Recall that the λ_c -contacts are characterized by a smooth dependence $F_s(u)$ as follows from the ME. The PN oscillations determine the lowest average kink velocity. Therefore, the lowest velocity allowed for the frictional crack propagation, $v_{k, \min}$, is

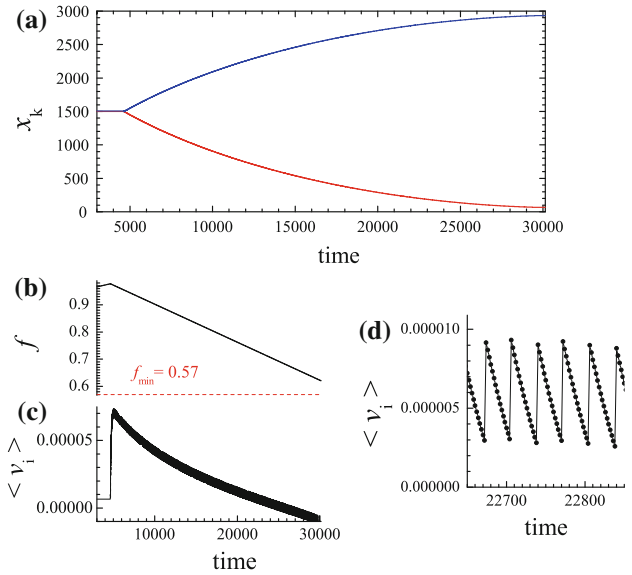


Fig. 7 (Color online) Evolution of the chain of $N = 3,000$ contacts. The nearest neighboring contacts interact elastically with the constant $g = 25$, the interaction with the substrate is modeled by the sawtooth function (35) with $k_c = 1$ and $u_c = 1$. All contacts are driven through the springs of the elastic constant $K = 0.07$, their ends moving with the velocity $v = 10^{-4}$. The motion is overdamped ($m = 1, \eta = 100$). To initiate the breaking, two central contacts interact with the substrate with smaller spring constants, $k'_c = 0.5$. When the kinks motion begins, the elastic constants of the central contacts restore their values to $k_c = 1$, and the driving velocity changes its sign, $v \rightarrow v_b = -2 \times 10^{-4}$. **a** shows the kinks centers (defined as places where the atomic velocity is maximal), **b** shows the driving force $f(t)$, **c** shows the average chain velocity $\langle \dot{u}_i \rangle = N^{-1} \sum_i \dot{u}_i$, and **d** demonstrates oscillation of the velocity due to PN barriers

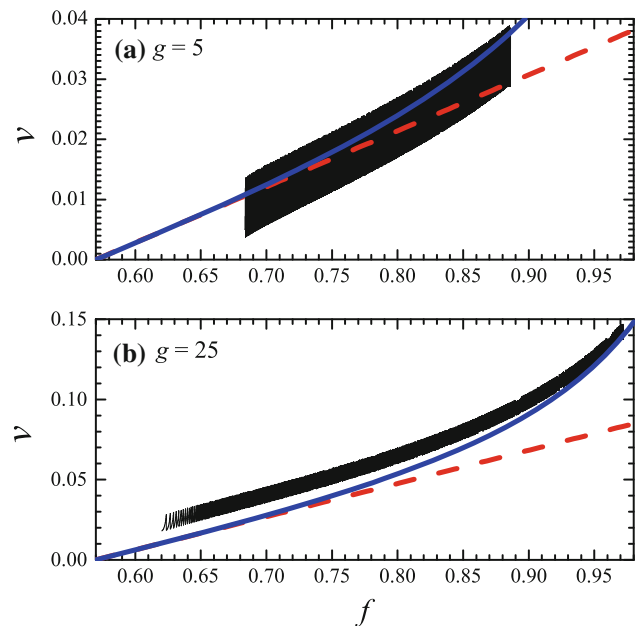


Fig. 8 (Color online) Kink velocity versus the driving force for **a** $g = 5 (v_b = -4 \times 10^{-5})$ and **b** $g = 25 (v_b = -2 \times 10^{-4})$; $N = 3 \times 10^4$, other parameters as in Fig. 7. *Blue solid and red dashed lines* correspond to Eqs. 40 and 43, correspondingly

determined by the parameters g and λ_c —the larger are g and λ_c , the smaller is $v_{k,\min}$.

5.2.4 Discussion

The FK–ME model used here is rather close to the well-known 1D Burridge–Knopoff (BK) model of earthquakes with a velocity-weakening friction law [35]. The difference is in the interface force $F_s(u)$: we use the function derived from the ME–EQ model (with well-defined parameters which may be extracted from experiments or calculated from first principles), whereas the BK model adopts a phenomenological velocity-dependent function for F_s . Nevertheless, the qualitative behavior of the two models is similar, the BK model also exhibits solitary-wave dynamics as was demonstrated numerically in Ref. [36]. In our case, however, by reducing the model to the FK–ME one, we can describe the solitary waves analytically and rigorously.

In the simulation we started from the well-defined initial configuration, when all contacts are relaxed except the one or two where kink's motion is initiated. If one starts from a random initial configuration, we expect that kinks will emerge at random places, so that several kinks may propagate through the system simultaneously, as was observed in simulation of the BK model [36].

Also we assumed that all λ_c -contacts are characterized by the same $F_s(u)$ dependence and thus have the same threshold values F_{th} . This is correct if the number of original contacts within a single λ_c -contact, $N_\lambda = (\lambda_c/a_c)^2$, is infinite. Otherwise, different λ_c -contacts will have different threshold values F_n , however, the distribution of their thresholds is narrower than the distribution of thresholds of single asperities by a factor $\sqrt{N_\lambda}$. A narrow distribution of thresholds will nevertheless have a qualitative effect because rupture fronts may stop when they meet λ_c -contacts with a threshold above the driving force. When the interface is disordered, the avalanches will have finite lengths and may become short for forces near f_{mi} , for which the rupture fronts propagate at the minimal velocity.

Our approach may also incorporate the existence of disorder and defects always present in real materials. On the one hand, defects may nucleate kinks (cracks); on the other hand, the kink propagation may be slowed down up to its complete arrest due to pinning by the defects. For example, the slowing down of the 1D crack propagating through a 2D system with quenched randomly distributed defects was considered in Ref. [37].

Thus, reducing the EQ–ME model of friction to the FK–ME one, we described avalanche-like dynamics of the frictional interface—the solitary wave of contacts breaking. If the force $F_s(u)$ has a sawtooth shape, then the interface

dynamics may be described analytically; otherwise one has to use numerics. The analogy with the FK model may be extended even further:

- The driven FK model exhibits hysteresis when the force increases and then decreases [24, 38]. The same effect was observed in the large-scale crack simulation [39], and thus could be observed in the frictional interface too.
- Effects of nonzero temperature may be considered. One may predict that at $T > 0$ the sliding kinks will experience an additional damping, while the immobile (e.g., arrested) kinks will slowly move (creep) due to thermally activated jumps.
- As shown in Refs. [24, 40], a fast driven kink begins to oscillate due to excitation of its shape mode, and then, with the further increase of driving, the kink is destroyed. This effect is similar to what is observed in fracture mechanics, where cracks begin to oscillate and then branch [41].
- If the interaction between the atoms is nonlinear and stiff enough, then the FK model admits the existence of supersonic kinks [42] which are similar to solitons of the Toda chain. It would be interesting to study if similar waves may appear in the frictional interface, as was predicted in crack propagation [43].
- One may suppose that the damping coefficient η in the equation of motion (34) depends on the kink velocity, $\eta(v)$. In fracture mechanics, this coefficient defines the rate at which the energy is removed from the crack edge, thus it plays a crucial role.
- A large number of studies are devoted to different generalizations of the FK model to 2D system (e.g., see [24]). For example, if kinks attract one another in the y (transverse) direction, then they unite into a line (dislocation) which moves as a whole (or due to secondary kinks).

6 Conclusion

We discussed the crucial role in sliding friction of the elastic interaction between the contacts at the inhomogeneous frictional interface and proposed various approaches to treat this problem from different viewpoints. The interaction produces a characteristic elastic correlation length $\lambda_c = a^2 E/k_c$. At distance $r < \lambda_c$, the slider may be considered as a rigid body but with a strong contacts' interaction, which leads to a shrinking of the effective contact-breaking threshold distribution and an enhanced possibility for a mechanical elastic instability to appear, which is conducive to stick slip. At large distances $r > \lambda_c$, the contact–contact interaction leads to screening of local

perturbations in the interface, or to appearance of collective modes (frictional cracks) propagating as solitary waves.

In this study, we assumed that the external stress (the driving force) is uniform across the system. In a general case, however, stress is nonuniform and may moreover change with (adjust itself to) interface dynamics, so that the problem should be considered self-consistently. For given boundary conditions, determined by the experimental setup, one should calculate the stress field, e.g., by finite element technique, which provides the driving force $f(r)$ in the FK–ME model. The latter defines the displacement field at the interface through the solution of the FK–ME master equations. The displacement field in turn is to be used as the boundary condition for the elastic-theory equations at the frictional interface (from other sides of the slider, the boundary conditions should correspond to a given experimental setup).

Acknowledgments The authors wish to express their gratitude to E.A. Jagla, B.N.J. Persson, M. Urbakh, and S. Zapperi for helpful discussions. This study was supported in part by CNRS-Ukraine PICS grant No. 5421, by ESF Eurocore FANAS AFRI through CNR-Italy, by PRIN/COFIN 20087NX9Y7, and by the SNF Sinergia Project NPA1617. O.B. acknowledges hospitality at SISSA and ICTP Trieste.

References

- Persson, B.N.J.: *Sliding Friction: Physical Principles and Applications*. Springer, Berlin (1998)
- Braun, O.M., Naumovets, A.G.: Nanotribology: microscopic mechanisms of friction. *Surf. Sci. Rep.* **60**, 79–158 (2006)
- Olami, Z., Feder, H.J.S., Christensen, K.: Self-organized criticality in a continuous, nonconservative cellular automaton modeling earthquakes. *Phys. Rev. Lett.* **68**, 1244–1247 (1992)
- Persson, B.N.J.: Theory of friction: Stress domains, relaxation, and creep. *Phys. Rev. B* **51**, 13568–13585 (1995)
- Braun, O.M., Röder, J.: Transition from stick-slip to smooth sliding: an earthquakelike model. *Phys. Rev. Lett.* **88**, 096102-1–4 (2002)
- Filippov, A.E., Klafter, J., Urbakh, M.: Friction through dynamical formation and rupture of molecular bonds. *Phys. Rev. Lett.* **92**, 135503-1–4 (2004)
- Farkas, Z., Dahmen, S.R., Wolf, D.E.: Static versus dynamic friction: the role of coherence. *J. Stat. Mech.: Theory and Experiment* P06015 (2005), and cond-mat/0502644
- Braun, O.M., Peyrard, M.: Modeling friction on a mesoscale: master equation for the earthquakelike model. *Phys. Rev. Lett.* **100**, 125501-1–4 (2008)
- Braun, O.M., Tosatti, E.: Kinetics of stick-slip friction in boundary lubrication. *Europhys. Lett.* **88**, 48003-1–6 (2009)
- Braun, O.M., Barel, I., Urbakh, M.: Dynamics of transition from static to kinetic friction. *Phys. Rev. Lett.* **103**, 194301-1–4 (2009)
- Braun, O.M., Peyrard, M.: Master equation approach to friction at the mesoscale. *Phys. Rev. E* **82**, 036117-1–19 (2010)
- Braun, O.M., Peyrard, M.: Dependence of kinetic friction on velocity: master equation approach. *Phys. Rev. E* **83**, 046129-1–9 (2011)
- Braun, O.M., Tosatti, E.: Kinetics and dynamics of frictional stick-slip in mesoscopic boundary lubrication. *Phil. Mag.* **91**, 3253–3275 (2011)
- Larkin, A.I., Ovchinnikov, Yu.N.: Pinning in type-II superconductors. *J. Low. Temp. Phys.* **34**, 409–428 (1979)
- Persson, B.N.J., Tosatti, E.: Theory of friction: elastic coherence length and earthquake dynamics. *Solid State Commun.* **109**, 739–744 (1999)
- Caroli, C., Nozieres, Ph.: Hysteresis and elastic interactions of microasperities in dry friction. *Eur. Phys. J. B* **4**, 233–246 (1998)
- Landau, L.D., Lifshitz, E.M.: *Theory of Elasticity*. Pergamon, New York (1986)
- Persson, B.N.J.: Theory of rubber friction and contact mechanics. *J. Chem. Phys.* **115**, 3840–3861 (2001)
- Persson, B.N.J., Bucher, F., Chiaia, B.: Elastic contact between randomly rough surfaces: comparison of theory with numerical results. *Phys. Rev. B* **65**, 184106-1–7 (2002)
- Persson, B.N.J.: On the elastic energy and stress correlation in the contact between elastic solids with randomly rough surfaces. *J. Phys. Condens. Matter* **20**, 312001-1–3 (2008)
- Yang, C., Persson, B.N.J.: Contact mechanics: contact area and interfacial separation from small contact to full contact. *J. Phys. Condens. Matter* **20**, 215214-1–13 (2008)
- Almqvist, A., Campañá, C., Prodanov, N., Persson, B.N.J.: Interfacial separation between elastic solids with randomly rough surfaces: comparison between theory and numerical techniques. *J. Mech. Phys. Solids* **59**, 2355–2369 (2011)
- Picard, G., Ajdari, A., Lequeux, F., Bocquet, L.: Elastic consequences of a single plastic event: a step towards the microscopic modeling of the flow of yield stress fluids. *Eur. Phys. J. E* **15**, 371–381 (2004)
- Braun, O.M., Kivshar, Yu.S.: *The Frenkel–Kontorova Model: Concepts, Methods, and Applications*. Springer, Berlin (2004)
- Sollich, P.: Rheological constitutive equation for a model of soft glassy materials. *Phys. Rev. E* **58**, 738–759 (1998)
- Hébraud, P., Lequeux, F.: Mode-coupling theory for the pasty rheology of soft glassy materials. *Phys. Rev. Lett.* **81**, 2934–2937 (1998)
- Bocquet, L., Colin, A., Ajdari, A.: Kinetic theory of plastic flow in soft glassy materials. *Phys. Rev. Lett.* **103**, 036001-1–4 (2009)
- Lemaître, A., Caroli, C.: Rate-dependent avalanche size in athermally sheared amorphous solids. *Phys. Rev. Lett.* **103**, 065501-1–4 (2009)
- Caroli, C.: Slip pulses at a sheared frictional viscoelastic/non-deformable interface. *Phys. Rev. E* **62**, 1729–1737 (2000)
- Gerde, E., Marder, M.: Friction and fracture. *Nature* **413**, 285–288 (2001)
- Greenwood, J.A.: The theory of viscoelastic crack propagation and healing. *J. Phys. D* **37**, 2557–2569 (2004)
- Greenwood, J.A.: Viscoelastic crack propagation and closing with Lennard–Jones surface forces. *J. Phys. D* **40**, 1769–1777 (2007)
- Vella, D., Boudaoud, A., Adda-Bedia, M.: Statics and inertial dynamics of a ruck in a rug. *Phys. Rev. Lett.* **103**, 174301-1–4 (2009)
- Braun, O.M., Peyrard, M.: Crack in the frictional interface as a solitary wave. *Phys. Rev. E* (submitted) (2011)
- Burridge, R., Knopoff, L.: Model and theoretical seismicity. *Bull. Seismol. Soc. Am.* **57**, 341–371 (1967)
- Schmittbuhl, J., Vilotte, J.-P., Roux, S.: Propagative macrodislocation modes in an earthquake fault model. *Europhys. Lett.* **21**, 375–380 (1993)
- Kierfeld, J., Vinokur, V.M.: Slow crack propagation in heterogeneous materials. *Phys. Rev. Lett.* **96**, 175502-1–4 (2006)
- Braun, O.M., Bishop, A.R., Röder, J.: Hysteresis in the underdamped driven Frenkel–Kontorova model. *Phys. Rev. Lett.* **79**, 3692–3695 (1997)
- Holland, D., Marder, M.: Ideal brittle fracture of silicon studied with molecular dynamics. *Phys. Rev. Lett.* **80**, 746–749 (1998)

40. Braun, O.M., Bambi, H.u., Zeltser, A.: Driven kink in the Frenkel–Kontorova model. *Phys. Rev. E* **62**, 4235–4245 (2000)
41. Fineberg, J., Marder, M.: Instability in dynamics fracture. *Phys. Rep.* **313**, 1–141 (1999)
42. Braun, O.M.: Supersonic and multiple topological excitations in the driven Frenkel–Kontorova model with exponential interaction. *Phys. Rev. E* **62**, 7315–7319 (2000)
43. Guozden, T.M., Jagla, E.A.: Supersonic crack propagation in a class of lattice models of mode III brittle fracture. *Phys. Rev. Lett.* **95**, 224302-1–4 (2005)